Kinetic dissection of pre-crRNA binding and processing by CRISPR-Cas12a

Selma Sinan, Nathan Appleby, Chia-Wei Chou, Ilya J. Finkelstein, and Rick Russell*

Supplementary Information

| | –34 Repeat Sequence | –15 Hairpin | 0 +1 Guide Sequence +24 |

–34 Repeat Sequence | **–15** Hairpin | **0 +1** Guide Sequence | **+24**

pre-crRNA(-34:+24)
GUCAAAAGACCUUUUUAAUUUCUACUCUUGUAGAUGUGAUAAGUGGAAUGCCAUGUGGA

-19d, pre-crRNA(-34:+24)
GUCAAAAGACCUUUUUAAUUUCUACUCUUGUAGAUGUGAUAAGUGGAAUGCCAUGUGGA

pre-crRNA(-23:+24)
UUUUUAAUUUCUACUCUUGUAGAUGUGAUAAGUGGAAUGCCAUGUGGA

-19d, pre-crRNA(-23:+24)
UUUUUAAUUUCUACUCUUGUAGAUGUGAUAAGUGGAAUGCCAUGUGGA

crRNA(-18:+24)
UAAUUUCUACUCUUGUAGAUGUGAUAAGUGGAAUGCCAUGUGGA

pre-crRNA(-34:0)
GUCAAAAGACCUUUUUAAUUUCUACUCUUGUAGAU

-19d, pre-crRNA(-34:0)
GUCAAAAGACCUUUUUAAUUUCUACUCUUGUAGAU

pre-crRNA(-23:0)
UUUUUAAUUUCUACUCUUGUAGAU

-19d, pre-crRNA(-23:0)
UUUUUAAUUUCUACUCUUGUAGAU

crRNA(-18:0)
UAAUUUCUACUCUUGUAGAU

Structured pre-crRNA(-34:+24)
GUCAAAAGACCUUUUUAAUUUCUACUCUUGUAGAUAUCAAGCCUUACGGUCACCGUAAC

pre-crRNA(-34:+10)
UUUUUAAUUUCUACUCUUGUAGAUGUGAUAAGUG

Target F pre-crRNA(-34:+24)
GUCAAAAGACCUUUUUAAUUUCUACUCUUGUAGAUAGGAUGAACAGUUCUGGCUGGAGU

U₂₀ guide pre-crRNA(-23:+20)
UUUUUAAUUUCUACUCUUGUAGAUUUUUUUUUUUUUUUUUUUUUUU

A₂₀ guide pre-crRNA(-23:+20)
UUCUUAAUUUCUACUCUUGUAGAUAAAAAAAAAAAAAAAAAAAA

U-rich tail pre-crRNA(-23:+31)
UUUUUAAUUUCUACUCUUGUAGAUGUGAUAAGUGGAAUGCCAUGUGGAUUUAUUU

DNA Chimeric Proximal-pre-crRNA(-23:+24)
UUUUUAAUUUCUACUCUUGUAGAUGTGATAAGTGGAAUGCCAG

DNA Chimeric Distal-pre-crRNA(-23:+24)
UUUUUAAUUUCUACUCUUGUAGAUGUGAUAAGUGGAATGCCATG

LbCas12a;pre-crRNA(-24:+24)
UUUUAAUUUCUACUAAGUGUAGAUGUGAUAAGUGGAAUGCCAUGUGGA

FnCas12a;pre-crRNA(-23:+24)
UUUUAAUUUCUACUGUUGUAGAUGUGAUAAGUGGAAUGCCAUGUGGA

I-R pre-crRNA(-22:+24)
UUUAAUUUCUACUGUUGUAGAUCCAGUCUAAAUCGCUUACUGGAGU

I-R pre-crRNA(-22:+29)
UUUAAUUUCUACUGUUGUAGAUCCAGUCUAAAUCGCUUACUGCGAAUUAGC

I-R pre-crRNA(-22:+31)
UUUAAUUUCUACUGUUGUAGAUCCAGUCUAAAUCGCUUACUGCGAUAUAGACG

I-pre-crRNA(-22:+24)
UUUAAUUUCUACUGUUGUAGAUACAGUAGAAAUUGCUUACUGGAGU

Figure S1. Sequences of pre-crRNAs and crRNAs used herein.

Blue letters indicate deoxyribose nucleotides. The arrow at the top depicts the cleavage position within the pre-crRNA. The underlined sequence within the construct named 'structured pre-crRNA(–34:+24)' is predicted to form a 6-bp stem with a 3-nt loop.
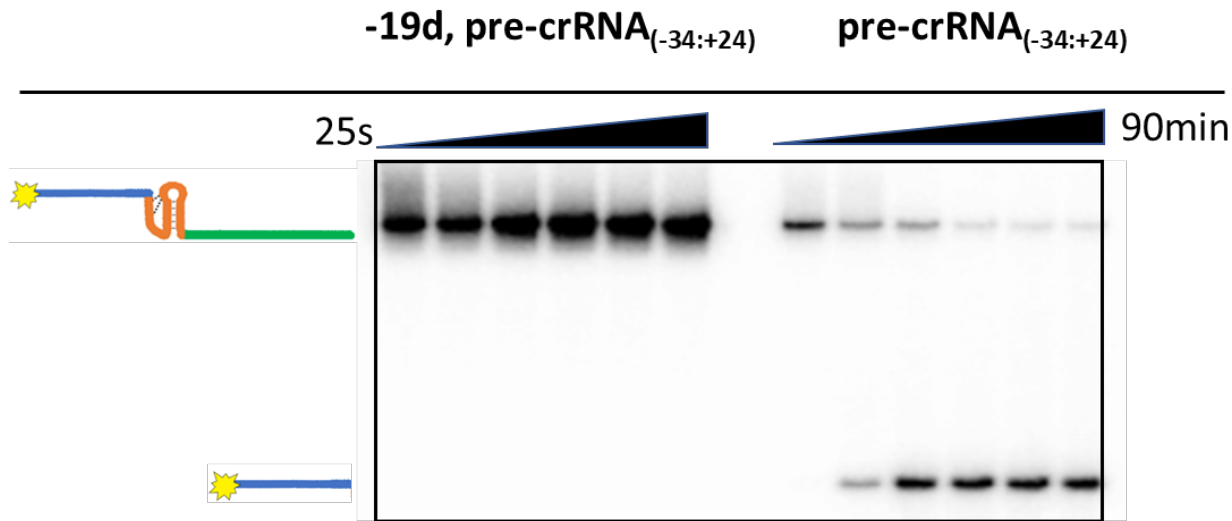
Figure S2. **Substitution of uridine(–19) with deoxyuridine (–19d, pre-crRNA$_{-34:+24}$) blocks RNA cleavage.**

Gel images are shown from reaction time courses for –19d, pre-crRNA$_{-34:+24}$ (left) and the all-ribose control, pre-crRNA$_{-34:+24}$ (right). Reactions included trace radiolabeled substrate (<1 nM) and 100 nM Cas12a. Aliquots were collected at reaction times of 25 s, 4 min, 20 min, 45 min, 65 min, and 90 min.
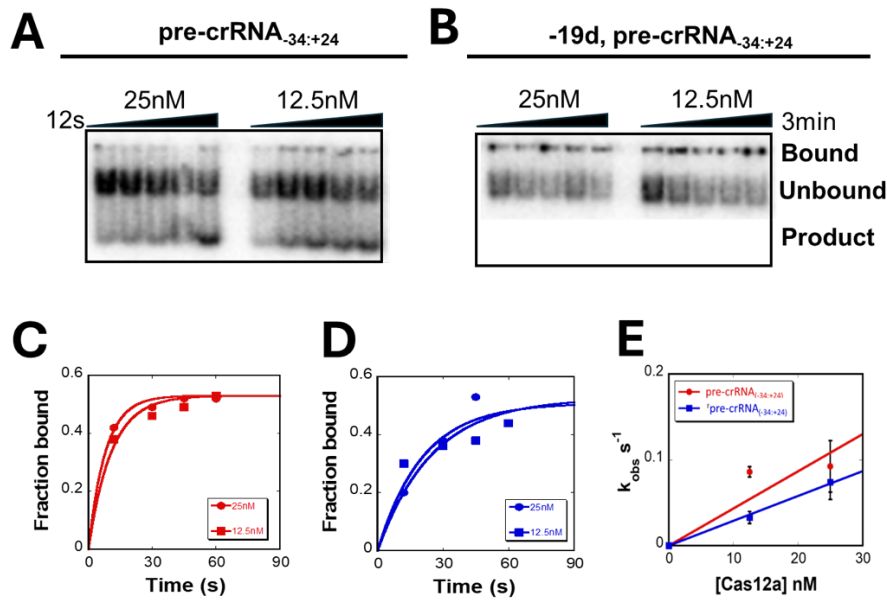
Figure S3. Substitution of U(−19) with deoxyuridine (−19d, pre-crRNA$_{-34:+24}$) has minimal effect on binding kinetics of the pre-crRNA

(A) Representative gel images of full-length pre-crRNA (pre-crRNA$_{-34:+24}$) binding time courses.

(B) Representative gel images of deoxyribose-substituted pre-crRNA (−19d, pre-crRNA$_{-34:+24}$) binding time courses.

(C) Quantitation of data from panel A (pre-crRNA$_{-34:+24}$). For each lane, the fraction of pre-crRNA that has bound to Cas12a was determined from the sum the intensities of the top and bottom bands (bound and cleaved, respectively) relative to the total intensity of the three bands.

(D) Quantitation of data from panel B (−19d, pre-crRNA$_{-34:+24}$). For each lane, the fraction of pre-crRNA bound to Cas12a was determined from the intensity of the top band (bound) relative to the total intensity of the two bands.

(E) Dependence of observed rate constant on Cas12a concentration. Binding rate constants determined from the slopes of the lines, in side-by-side experiments, were 4.3 ($\pm$ 0.6) $\times$ 10^6 M^{-1} s^{-1} and 2.9 ($\pm$ 0.4) $\times$ 10^6 M^{-1} s^{-1} for pre-crRNA$_{-34:+24}$ and −19d, pre-crRNA$_{-34:+24}$, respectively, reflecting the average and SEM from three independent experiments.

Binding reactions were performed under standard conditions (see Methods) except that the buffer was 50 mM Na-MES, pH 6.0 to reduce cleavage of the all-RNA pre-crRNA. This change had little or no effect on the binding kinetics of the all-ribose pre-crRNA (see Table 1). Unbound, bound, and cleaved pre-crRNA were resolved by native PAGE (see Methods).
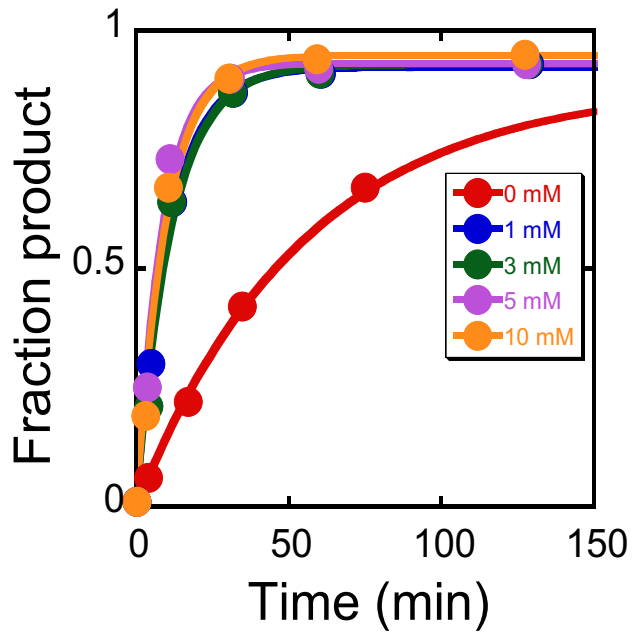
Figure S4. Pre-crRNA cleavage depends weakly on the presence of Mg^{2+}

Reactions included 50 nM Cas12a, trace labeled pre-crRNA$_{-34:+24}$, and no Mg^{2+} (red) or various Mg^{2+} concentrations (colors as indicated). For the reaction without Mg^{2+}, 10 mM EDTA was included to ensure the absence of free Mg^{2+}. Time course data were fit by a first-order rate equation. Rate constants were determined from the reactions shown and 2-4 additional replicates and were 3.0 (±0.5) × 10^{-4} s^{-1} in the absence of Mg^{2+}, 1.5 (±0.1) × 10^{-3} s^{-1} with 1 mM Mg^{2+}, 1.4 (±0.3) × 10^{-3} s^{-1} with 3 mM Mg^{2+}, 1.9 (±0.1) × 10^{-3} s^{-1} with 5 mM Mg^{2+}, and 1.7 (±0.2) × 10^{-3} s^{-1} with 10 mM Mg^{2+} (average ± SEM).
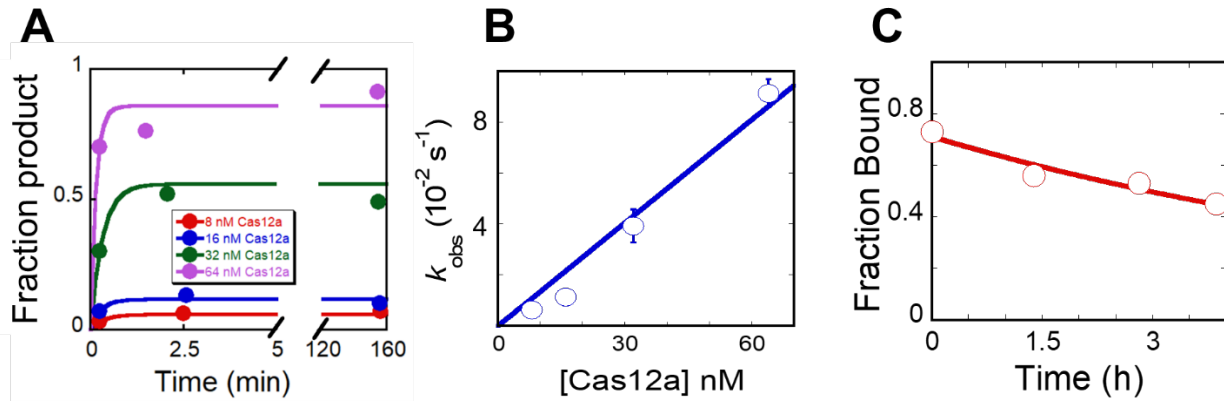
Figure S5. Binding and Dissociation kinetics of pre-crRNA$_{-34:+24}$ in the absence of Mg^{2+}.

(A) Binding time courses. Cas12a was present at the indicated concentrations, and pre-crRNA$_{-34:+24}$ was present at a trace concentration (<2 nM). Data were fit by a pseudo-first-order rate equation to yield observed rate constants at each Cas12a concentration.

(B) The observed rate constants from data in panel A and 3-5 additional replicate data are plotted against Cas12a concentration (points reflect average ± SEM). The data from each experiment were fit by a line, with the slope giving a k_{on} value of 1.4 (±0.4) × 10^6 M^{-1} s^{-1}.

(C) Time dependence for dissociation of pre-crRNA$_{-34:+24}$ in the absence of Mg^{2+}. Data were fit by a first-order rate equation, with the endpoint forced to the value obtained in a control reaction in which the labeled and unlabeled oligonucleotides were pre-mixed and then added to Cas12a. The fit from the data shown and three additional determinations gave a k_{off} value of 3.2 (±1.5) × 10^{-5} s^{-1} (average ± SEM).
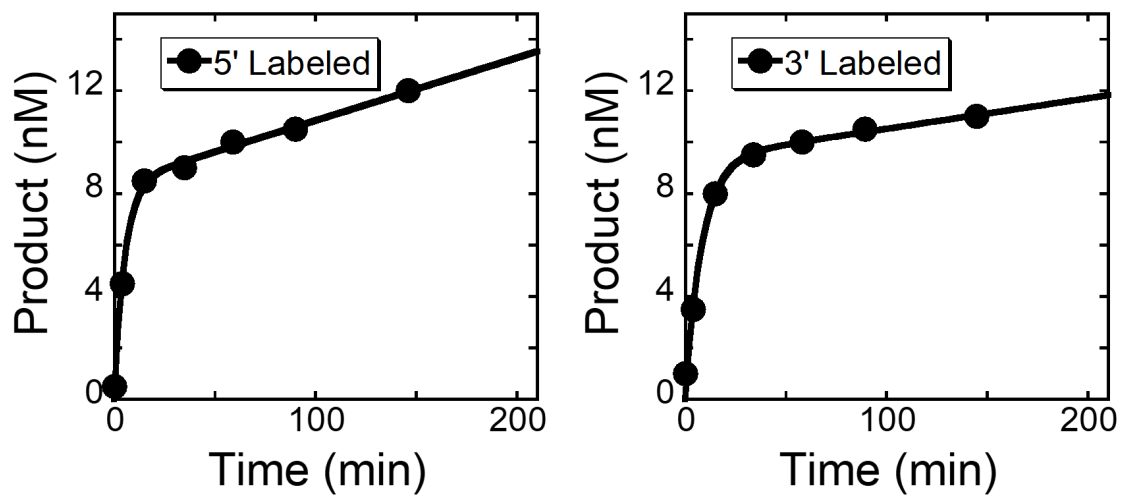
Figure S6. Dissociation kinetics of mature crRNA measured by multiple turnover processing of pre-crRNA$_{-34:+24}$.

Reactions included 10 nM Cas12a and 50 nM pre-crRNA$_{-34:+24}$ that was radiolabeled at the 5' end (left panel) or the 3' end (right panel). The slopes in the slow phase, which reflect the rate constants for release of the product crRNA, were 2.2 ($\pm$0.3) $\times$ 10^{-5} s^{-1} and 1.0 ($\pm$0.02) $\times$ 10^{-5} s^{-1} for the 5'-labeled and 3'-labeled pre-crRNA, respectively (average $\pm$ SEM from three independent replicates). Note that for the 5'-labeled pre-crRNA, the label is on the upstream sequence, which dissociates rapidly and does not contribute to the measured rate. Thus, this experiment measures dissociation of the unlabeled mature crRNA (left) or the 3'-labeled mature crRNA (right).
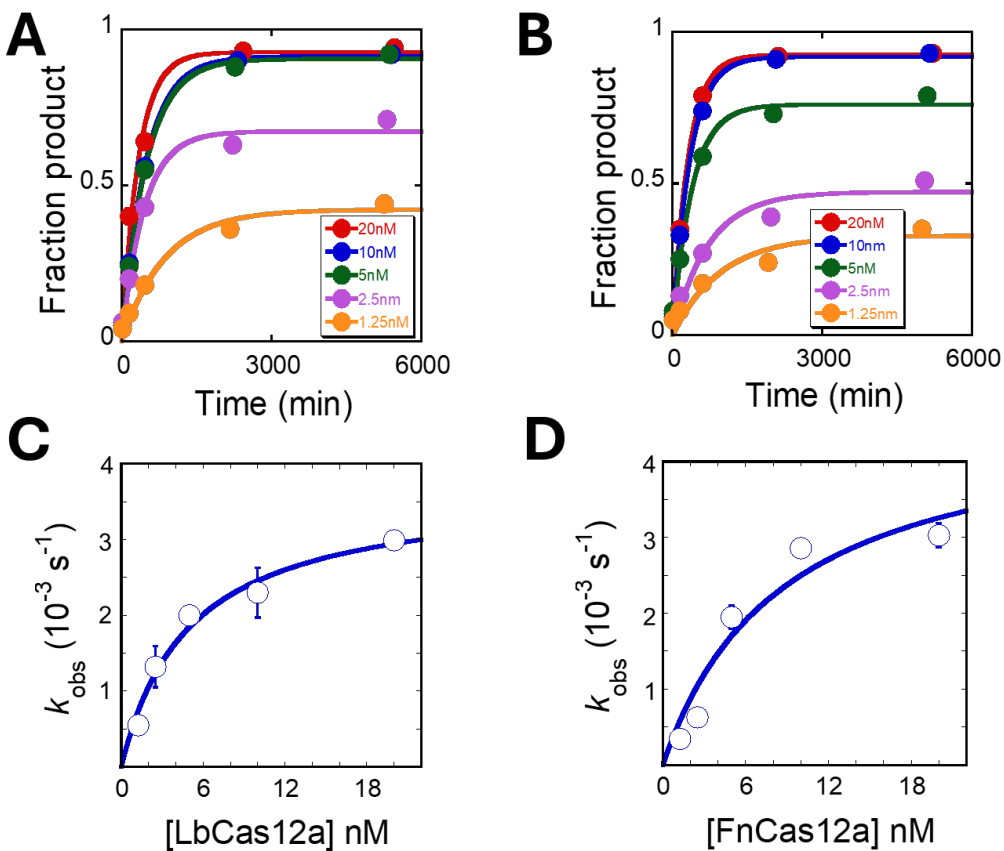
Figure S7. Pre-crRNA binding and processing kinetics of LbCas12a and FnCas12a.

(A) Pre-crRNA processing time courses for LbCas12a. LbCas12a was present at the indicated concentrations, and pre-crRNA was present at a trace concentration (<2 nM; see Table S1 for pre-crRNA sequence). Cleaved and uncleaved pre-crRNA were resolved by denaturing PAGE as for AsCas12a reactions.

(B) Pre-crRNA processing time courses for FnCas12a. FnCas12a was present at the indicated concentrations, and pre-crRNA was present at a trace concentration (<2 nM; see Table S1 for pre-crRNA sequence). Cleaved and uncleaved pre-crRNA were resolved by denaturing PAGE as for AsCas12a reactions.

(C) Concentration dependence of the observed rate constant for LbCas12a. Data from three independent measurements were fit by a hyperbola, giving a second-order rate constant of 8.1 ($\pm$0.4) $\times$ 10^5 M^{-1} s^{-1} (average $\pm$ SEM).

(D) Concentration dependence of the observed rate constant for FnCas12a. Data from three independent measurements were fit by a hyperbola, giving a second-order rate constant of 5.4 ($\pm$0.3) $\times$ 10^5 M^{-1} s^{-1} (average $\pm$ SEM).
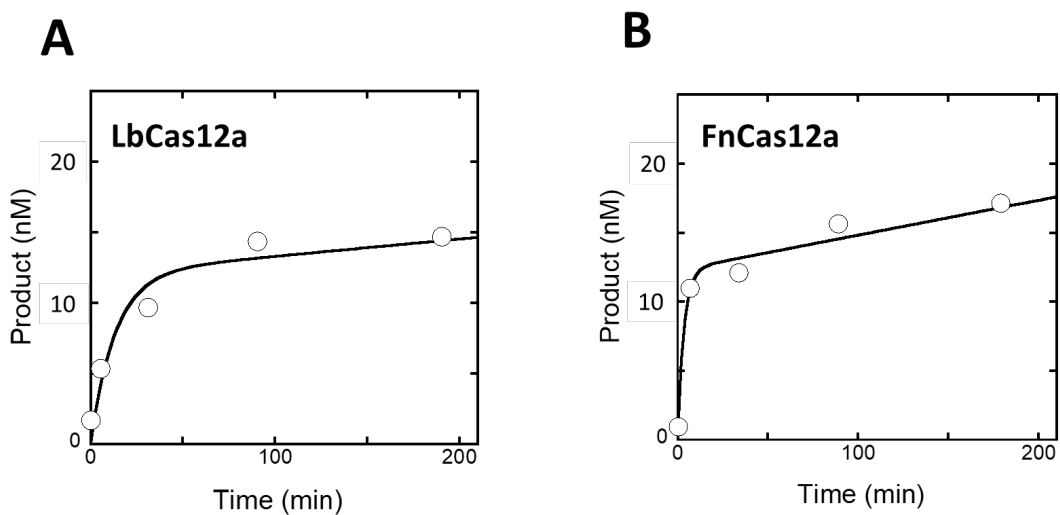
Figure S8. Dissociation kinetics of mature crRNA measured by multiple turnover processing of pre-crRNA by LbCas12a and FnCas12a

Reactions were conducted with 10 nM Cas12a and 50 nM pre-crRNA for LbCas12a (panel A) and FnCas12a (panel B), respectively (see Table S1 for pre-crRNA sequences). The slow phase slopes, representing the rate constants for product crRNA release, were 2.4 ($\pm$0.4) $\times$ 10^{-5} s^{-1} for LbCas12a and 1.7 ($\pm$0.7) $\times$ 10^{-5} s^{-1} for FnCas12a from the average $\pm$ SEM from three replicate measurements for each enzyme.
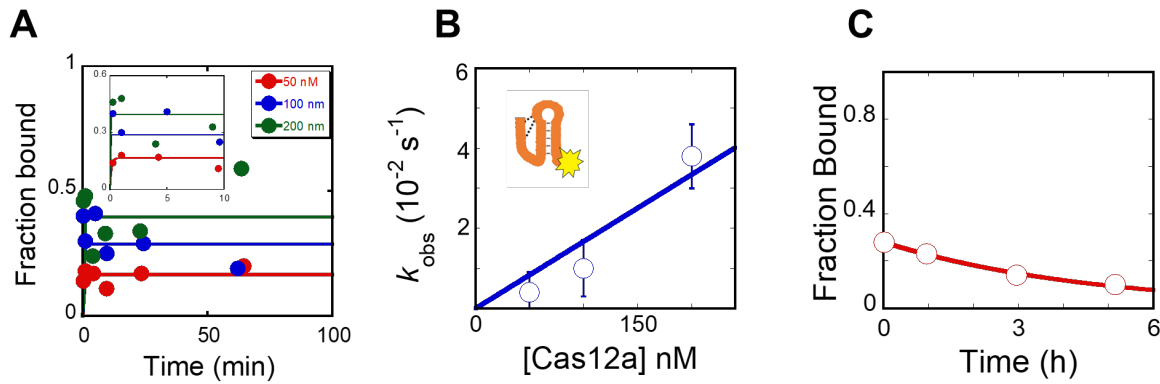
Figure S9. Binding and dissociation kinetics of the crRNA lacking the guide sequence (crRNA$_{-18:0}$).

(A) Binding time courses. Cas12a was present at the indicated concentrations, and crRNA$_{-18:0}$ was present at a trace concentration (<2 nM). The inset shows the data at the early time points. At the relatively high protein concentrations that were necessary to detect significant binding, equilibration was complete or nearly complete by the first time point, as shown. Nevertheless, calculation of the binding rate constant using only the lowest protein concentration, which gave the most significant increase in binding at the early times, gives essentially the same rate constant, and the relatively low endpoints reinforce the conclusion of greatly weakened binding for this construct, driven both by slower binding and by faster dissociation (panel C).

(B) The observed rate constant from data in panel A and two additional replicate datasets are plotted against Cas12a concentration. Error bars reflect the SEM from the rate constants determined at each Cas12a concentration. Plots of the rate constants from the three individual experiments were fit by a line, giving a binding rate constant of 1.7 ($\pm$0.2) $\times 10^5$ (average $\pm$ SEM of rate constants determined from each experiment).

(C) Time dependence of crRNA$_{-18:0}$ dissociation from Cas12a. These data and plots from five independent experiments were fit by a first-order rate equation, giving a rate constant of 6.7 ($\pm$0.2) $\times 10^{-5}$ s^{-1} (average $\pm$ SEM).
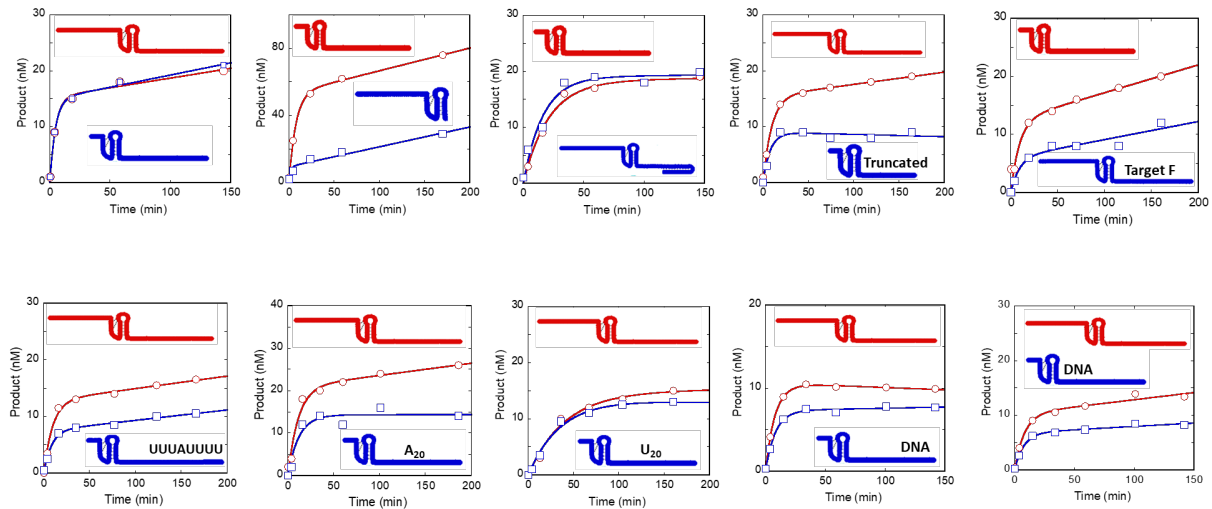
Figure S10. Relative binding rate constants for pre-crRNA variants measured by competition for Cas12a

Reactions included a pre-crRNA variant to be measured, as depicted by the blue cartoons, and a reference pre-crRNA (red cartoon). The relative binding rate constants are determined by the relative amplitudes of product formation in the 'burst' phase. In each reaction, the reference crRNA was chosen such that the product lengths would be different from the variant pre-crRNA being tested. These two pre-crRNAs were used as equivalent references because they were shown to react equivalently to each other (top left). For most reactions, the Cas12a concentration was 50 nM (active concentration approximately 20 – 30 nM), and each substrate was 50 nM. In the reaction at top left, each substrate concentration was 100 nM, and the top row, second from left, included 100 nM Cas12a (40 – 60 nM active Cas12a) and 100 nM of each substrate.
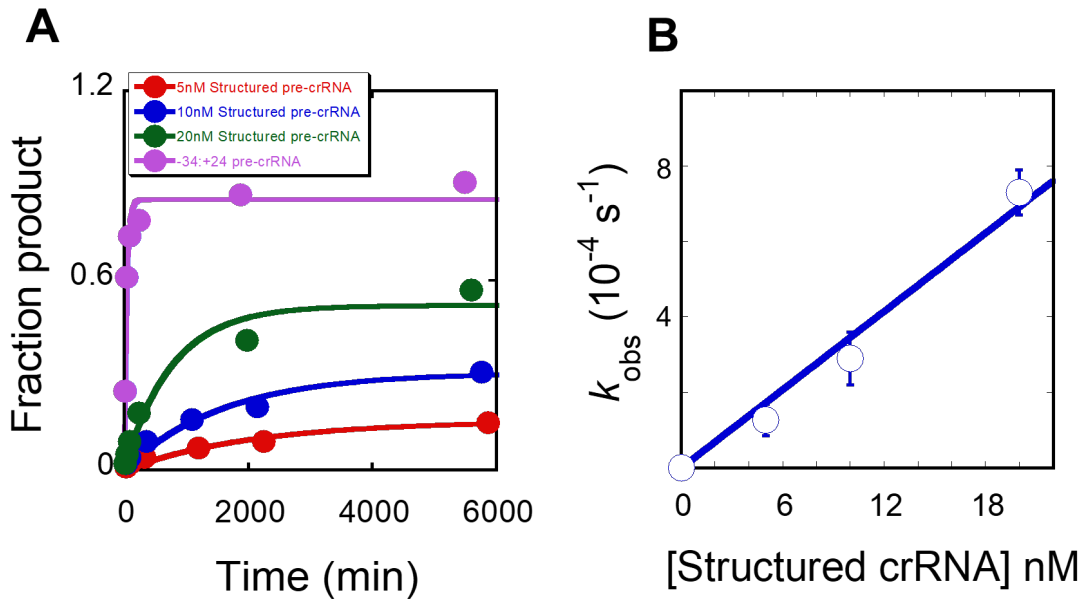
Figure S11. Inhibition of DNA targeting by crRNA with potential for stable hairpin formation in the guide region

The second-order rate constant for DNA targeting was determined by measuring DNA non-target strand cleavage under conditions of subsaturating Cas12a RNP. This second-order rate constant reports on the DNA binding rate constant for standard Cas12a-crRNA complexes (Strohkendl et al. 2018), and we infer that the decreased rate constant for the crRNA here reflects slowed DNA binding due to inhibition of complete R-loop formation. After complete R-loop formation, we hypothesize that non-target strand cleavage proceeds normally, as the hairpin in the crRNA would be removed by R-loop formation, but the data leave open the possibility of effects on this rate constant in addition to, or instead of, effects on the binding rate constant.

(A) Time courses of DNA targeting measured by non-target strand cleavage. The structured pre-crRNA was incubated at the indicated concentrations with 60 nM Cas12a for 30 min at 25 °C to allow assembly and processing to the mature RNP. The standard crRNA (crRNA$_{-34:+24}$) was also tested side-by-side as a control (20 nM pre-crRNA; orange).

(B) The dependence of the observed rate constant for nontarget strand cleavage is plotted against the pre-crRNA concentration. The data gave a second-order rate constant for DNA targeting of 4.8 ($\pm$1.0) $\times$ 10^4 M^{-1} s^{-1}, a decrease of ~1000-fold relative to the standard pre-crRNA and matched target DNA (violet in panel A).
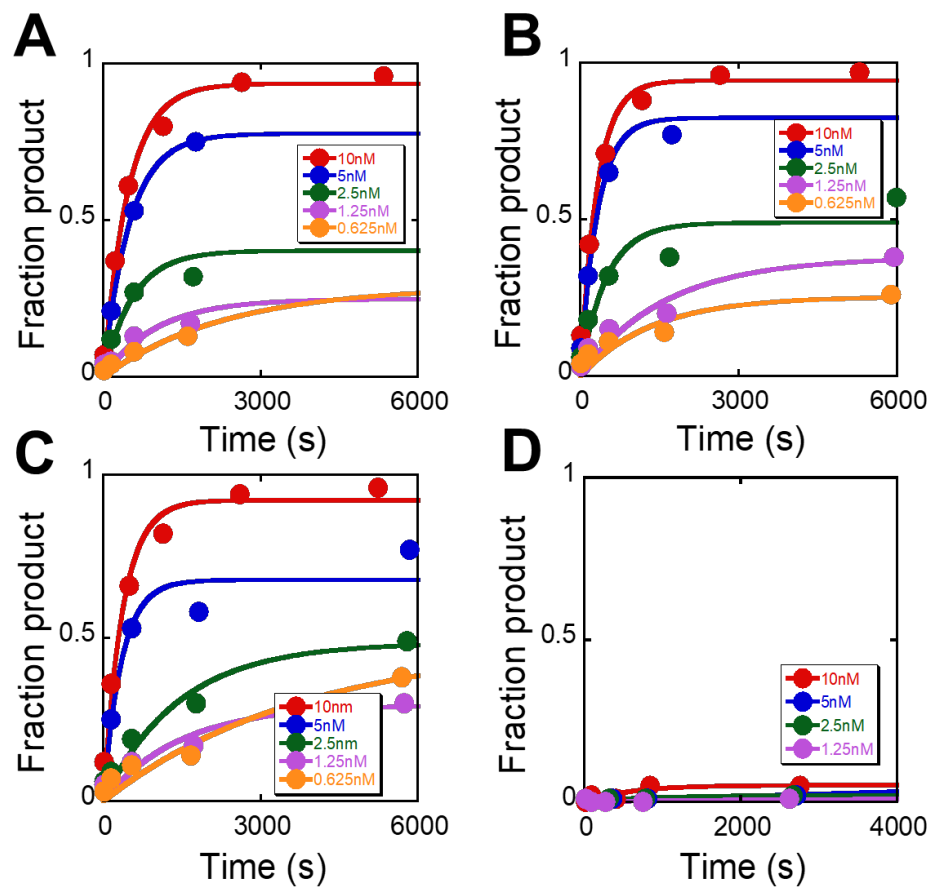
Figure S12. Time courses for Cas12a-mediated processing reactions of pre-crRNAs that include potential for inhibitory secondary structure

Cas12a was present at the indicated concentrations, and pre-crRNAs were present at a trace concentration (<2 nM). Plots of the observed rate constants vs Cas12a concentration, used to generate values of k_{on}, are in Fig. 7B.

(A) Time courses for inhibition/rescue (I-R) pre-crRNA$_{-22:+24}$

(B) Time courses for I-R pre-crRNA$_{-22:+29}$

(C) Time courses for I-R pre-crRNA$_{-22:+31}$

(D) Time courses for I-pre-crRNA$_{-22:+24}$